# Safer Batteries through Coupled Multiscale Modeling

John Turner, Srikanth Allu, Mark Berrill, Wael Elwasif,
Sergiy Kalnaus, Abhishek Kumar, Damien Lebrun-Grandie,
Sreekanth Pannala, and Srdjan Simunovic
*Oak Ridge National Laboratory, Oak Ridge, TN, U.S.A.*
turnerja@ornl.gov

**Abstract**
Batteries are highly complex electrochemical systems, with performance and safety governed by coupled nonlinear electrochemical-electrical-thermal-mechanical processes over a range of spatiotemporal scales. We describe a new, open source computational environment for battery simulation known as VIBE - the Virtual Integrated Battery Environment. VIBE includes homogenized and pseudo-2D electrochemistry models such as those by Newman-Tiedemann-Gu (NTG) and Doyle-Fuller-Newman (DFN, a.k.a. DualFoil) as well as a new advanced capability known as AMPERES (Advanced MultiPhysics for Electrochemical and Renewable Energy Storage). AMPERES provides a 3D model for electrochemistry and full coupling with 3D electrical and thermal models on the same grid. VIBE/AMPERES has been used to create three-dimensional battery cell and pack models that explicitly simulate all the battery components (current collectors, electrodes, and separator). The models are used to predict battery performance under normal operations and to study thermal and mechanical response under adverse conditions.

*Keywords:* battery safety, coupled physics, electrochemistry, energy storage, multiphysics, multiscale

# 1 Introduction

Most high-capacity rechargeable Lithium-ion batteries (LIBs) in mobile power applications (vehicles, tools, phones, etc.) are based on intercalation reactions in which the mobile cations are inserted into a host structure of electrodes. A typical Li-ion cell sandwich consists of positive (cathode during discharge) and negative (anode during discharge) porous composite insertion electrodes, a porous separator, negative (copper) and positive (aluminum) current collectors. The amount of energy stored in a battery is directly proportional to the amount of active material that moves back and forth between the electrodes. Battery power is limited by (1) the rate of diffusion of Li cations into cathode or anode particles, (2) the electrical conductivity of cathode materials, and (3) the rate and distance of ionic transport in the electrolyte and between the electrode particles. Any mismatch in the transport across the scales can cause local temperature excursions and heterogeneities of the chemical species

that can result in catastrophic failure, such as explosion of this hazardous mix of fuel and oxidizer (analogous to solid propellants).

Repeated charging and discharging degrades a Li-ion battery, affecting its chemical and structural stability, capacity, voltage, power, and safety. Further improvements in the battery performance will require addressing both materials science and chemistry challenges [1]. At the device level, scale-up and integration of LIB unit cells into battery packs for vehicle powertrains [2] involve system power and thermal management, abuse tolerance, and safety. Temperature imbalance can lead to shortened life; and in the extreme case, temperatures in excess of 90$^{o}$C can trigger exothermic chemical reactions initiated by metastable SEI layers that can lead to cell thermal runaway [3-5]. Thermal excursion can be especially severe when a cell is unintentionally shorted or otherwise abused.

Mechanical deformation [6] of batteries can trigger thermal runaway events by causing rearrangement of electrode material, transfer of normal and shear stresses to the separator, and eventually rupture of the separator and short circuits [7]. The electrical contacts and the subsequent thermal runaway event will depend on the contact area, contact resistance, cell capacity, and the ability of the current flow through the short to generate sufficient heat to cause the local temperature to rise above ~90$^{o}$C to trigger the thermal runaway events.

Given these complex options for chemistry and materials, it is important to have a simulation capability and models that can predict performance, design and support experiments, optimize material components and geometries, and estimate safety and durability in an integrated fashion [8].

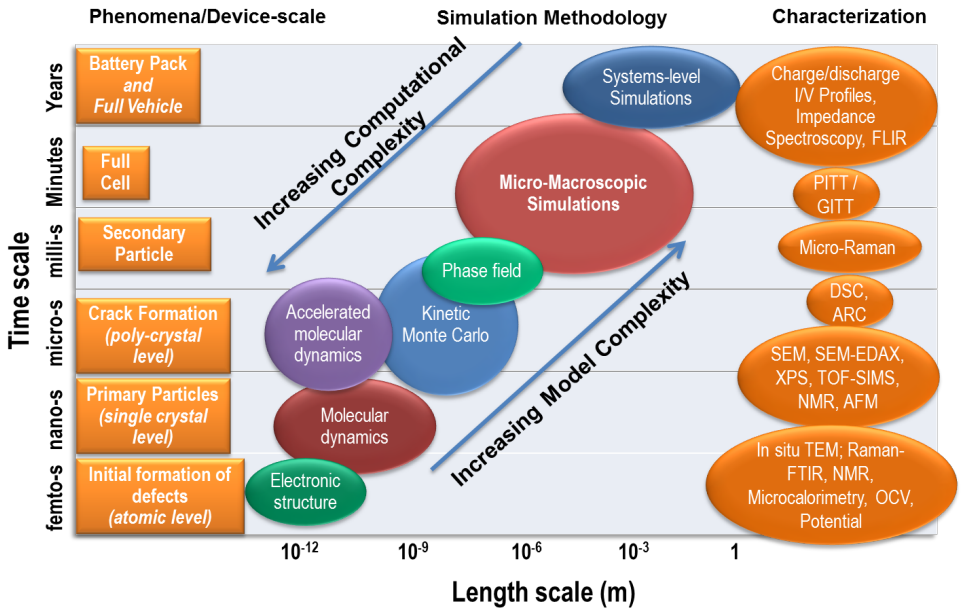


**Figure 1. Multiscale and multiphysics models for batteries and electrochemical systems resolving the processes occurring at different scales, along with corresponding characterization techniques.**

Figure 1 shows the computational methods available for modeling and simulation of batteries, electrochemical systems and materials at various length and time-scales, which can be summarized as:

- Electronic structure methods for modeling the atomistic structures and properties [8] that provide fundamental insight into the atomistic and electronic processes governing energy and power densities, as well as structural integrity;
- Classical force-field methods for the dynamics and structure of materials [9,10], which are used to study defect formations and evolution;

- Kinetic Monte Carlo (KMC) for modeling electrochemical reactions [11] in interfacial chemistry
- Phase field method [12-14] for modeling mesoscopic transport of ions and species in order to understand the various resistances at the secondary particle level and optimize the chemistry;
- Coupled micro-macroscopic models to simulate spatiotemporally varying fields, such as ions and species [15-17] at the cell/electrode levels to optimize safety and performance;
- Macroscopic and/or system-level models [18-29] for simulation of full cells and battery packs, including life prediction and abuse scenarios.

To date, battery simulations have relied heavily on simplified unit cell models (e.g., 1-D and pseudo-2D) and equivalent circuit models to account for cell performance variations [4,30,31] thereby ignoring the underlying cell-to-cell electrochemical and thermal coupling. Following a description of the underlying physics models for electrochemical systems in Section 2, we describe the new simulation system VIBE - the Virtual Integrated Battery Environment [32]. While VIBE is targeted at time and length-scales at the mesoscale and above, integration of components with a range of fidelity provides researchers with a tool to accurately and efficiently explore problems ranging from the effects of crystallographic texture in electrodes on cell performance to simulation of deformation and internal short circuits.

# 2 Physics Models

In this section we describe models for the four major physical phenomena in Li-ion batteries: (a) electro-chemistry, (b) electronic transport, (c) heat transport, and (d) mechanics. The electro-chemistry model acting over the electro-active components provides heat source and electrical resistance but requires temperature, geometry, stress, current, etc. from other components. The electrical component acting over the entire device needs resistance and geometry but provides current, heat source, etc. The thermal component acting over the entire domain needs heat sources, geometry but provides temperature. The mechanical component takes temperature and provides deformed geometry/stress etc. If the processes are separated in spatiotemporal scales, one can perform loose coupling and obtain accurate solutions. However, in reality the scales overlap and one needs the ability to couple these models to accurately predict response.

## 2.1 Electrochemistry

Several models applicable to redox-based energy storage systems have been developed with different degrees of complexity and idealization. In the most general form, the mass and charge conservation in 3D can be described with four differential equations applicable to host material (subscript *s*) and electrolyte (subscript *e*) phases [15,33].

$$\begin{cases} \dfrac{\partial(\varepsilon_e c_e)}{\partial t} = \nabla\cdot\left(D_e^{eff}\nabla c_e\right) + \dfrac{1-t_+^0}{F} j^{Li} \\ \dfrac{\partial(\varepsilon_s c_s)}{\partial t} = \nabla\cdot\left(D_s^{eff}\nabla c_s\right) - \dfrac{j^{Li}}{F} \end{cases} \qquad (1)$$

$$\begin{cases} \nabla\cdot\left(\kappa^{eff}\nabla\varphi_e\right) + \nabla\cdot\left(\kappa_D^{eff}\nabla\ln(c_e)\right) = -j^{Li} \\ \nabla\cdot\left(\sigma^{eff}\nabla\varphi_s\right) = j^{Li} \end{cases} \qquad (2)$$

where $c_s$ and $c_e$ are solid and electrolyte lithium concentrations, $\varphi_s$ and $\varphi_e$ are solid and electrolyte potentials, $F$ is the Faraday constant, and $t_+^0$ is the cation transference number in the electrolyte. Conservation of species (Eq. 1) and conservation of charge (Eq. 2) are connected via flux of charge

associated with lithium ions $j^{Li}$. The latter is described by the Butler-Volmer equation of cathodic (anodic) reaction at the interface

$$j^{Li} = \frac{i_0}{F}\left[ exp\left(\frac{\alpha_a F}{RT}\eta\right) - exp\left(-\frac{\alpha_c F}{RT}\eta\right)\right] \tag{3}$$

which is driven by the local overpotential $\eta = \varphi_s - \varphi_e - U$, with $U$ being the open circuit potential of a particular half-cell reaction under consideration. The exchange current density $i_0$ is a function of lithium concentration

$$i_0 = k c_e^{\alpha_a}\left(c_{s,\max} - c_s\right)^{\alpha_a} c_s^{\alpha_c} \tag{4}$$

where $c_{s,\max}$ is the maximum stoichiometric content of Li in the host electrode material.

Effective solid and electrolyte transport properties, i.e., diffusivities ( $D_s^{eff}$ and $D_e^{eff}$ correspondingly) and conductivities ( $\sigma^{eff}$ and $k^{eff}$ ) are described in terms of corresponding volume fractions $\varepsilon_s$ and $\varepsilon_e$ as exponential relationships of a general form $\Theta^{eff} = \varepsilon^p \Theta$. Exponent $p$ could be taken as Bruggeman coefficient of 1.5 or used as an adjustable parameter to fit the discharge curve data [34]. The diffusional conductivity $\kappa_D^{eff}$ is determined following the concentrated solution theory [35] as

$$\kappa_D^{eff} = \frac{2RT\kappa^{eff}}{F}\left(t_+^0 - 1\right)\left(1 + \frac{d\ln f_\pm}{d\ln c_e}\right) \tag{5}$$

where $f_\pm$ is the mean molar activity coefficient of the electrolyte.

Equations 1 and 2 describe the mass and charge balances in electrode and electrolyte domains of a redox cell in three dimensions. Several simplifications to this general model have been proposed. One of the more well-known approaches is the pseudo-2D model developed by Doyle, Fuller, and Newman [34-36]. The model, sometimes referred to as the DFN model, is based on porous electrode theory and casts the equations of diffusion and charge transfer onto a simplified geometry. This geometry is described by two coordinates – one through the electrode thickness and the other being radial coordinate of an electrode particle idealized as a sphere. Transport through the electrolyte is modeled by using the concentrated solution theory and the pore-wall flux of lithium ions across the electrode-electrolyte interface is naturally set to zero in the separator region of the cell sandwich while at the active material interface it follows the Butler-Volmer equation. With such a simplification, solid state diffusion reduces to a 1D equation in the radial coordinate *r* of a particle with radius $R_s$

$$\frac{\partial c_s}{\partial t} = D_s\left(\frac{\partial^2 c_s}{\partial r^2} + \frac{2}{r}\frac{\partial c_s}{\partial r}\right) \tag{6}$$

In order to reduce compute time, Eq. 6 can be solved either by the Duhamel superposition method [35] or by using approximations for the surface lithium concentration that come from the diffusion length formulas derived by C.Y. Wang et al. [15]. In the latter case the approximation for surface concentration can be expressed as [37]

$$c_s = c_{avg} + \frac{j^{Li} l_s}{F D_s}\left[1 - \exp\left(-\frac{4}{3 l_s}\sqrt{D_s t}\right)\right] \tag{7}$$

where $l_s = R_s/5$ is the diffusion length corresponding to a spherical geometry with radius $R_s$. With such a description, the initial surface concentration is equal to the average concentration of lithium in the solid and approaches a linear asymptote at long discharge/charge times of $c_{avg} + \frac{j^{Li} l_s}{F D_s}$.

The second category of electrochemical models is based on a description of cell behavior from experimentally measured impedance characteristics. The model was developed by Newman, Tiedemann [38] and Gu [39] and accordingly is commonly referred as the NTG model. The cell current density ($J$) is linearly related to the cell potential ($V$) as

$$J = Y(V - U) \tag{8}$$

where $Y$ and $U$ represent the effective conductance and the open circuit potential (OCP) of the cell respectively. They are expressed as polynomial functions of state of charge variable $\theta$

$$\begin{cases} U = \sum_{i=0}^{N} a_i \theta^i \\ Y = \sum_{i=0}^{M} b_i \theta^i \end{cases} \tag{9}$$

The degree of polynomial ($N$) and the values of constants $a_i$ and $b_i$ are determined from the cell discharge curves for a number of C-rates. When the cell potentials are plotted versus applied current density, the cell voltages at zero current represent the OCPs of the cell and the slopes of potentials represent the cell impedance $1/Y$. Linear dependence of the latter on the current density is assumed, resulting in $Y$ being a function of state of charge only. While the NTG model allows rapid simulation of large systems (modules or packs), it provides only overall cell response, and hence cannot be used in situations where local variations in species or effects are of interest.

We are also developing an advanced electrochemistry capability known as AMPERES [5,32,40] (Advanced MultiPhysics for Electrochemical and Renewable Energy Storage). AMPERES uses a volume-averaged formulation that preserves the full 3D treatment of equations (1) and (2) and fully couples electrochemistry with electrical and thermal models on the same grid.

## 2.2 Electronic transport

The conservation of charge within the cell (or module or pack) is expressed by the Laplace equation:

$$\nabla(\sigma \nabla V) = 0 \tag{10}$$

over the entire union of cell sandwich, current collector, and electrical interconnect component domains. A non-singularity of electric field and conservation of charge is imposed on a single 3D domain with appropriate boundary conditions applied to the current collector tabs. The values of conductivity $\sigma$ of the cell sandwich are determined as a result of the solution of the corresponding electrochemical set of equations.

## 2.3 Heat transport

In its general form the three-dimensional heat conduction equation is expressed as

$$\rho C_p \frac{\partial T}{\partial t} - \nabla(k \nabla T) = q \tag{11}$$

where $\rho$ is the density, $C_p$ is the specific heat capacity, $k = \{k_x, k_y, k_z\}$ is the anisotropic thermal conductivity, and $T$ is local temperature. In Li-ion battery cells, thermal properties are highly anisotropic due to their layered cell structure. Equation 11 is solved for the entire cell, module, and pack. In electrical interconnect components and current collectors heat source is represented by a simple ohmic heating model. The heat generation model within the electrochemical dual-electrode cells was derived by Bernardi et al. [41]. In its simplified form commonly employed in battery simulations, the heat generation consists of irreversible energy loss due to cell polarization, reversible entropy change due to particular half-cell reaction and ohmic heating within cell sandwich.

$$q = \sum_j a_j i_j \left(\phi_s - \phi_e - U_j\right) + \sum_j a_j i_j T \frac{\partial U_j}{\partial T} + \frac{(i_s)^2}{\sigma^{eff}} \tag{12}$$

where the summation in general occurs over all reactions $j = 1...M$ which in case of Li-ion intercalation systems simplifies to two half-cell reactions at each electrode with corresponding OCP vs. lithium being denoted as $U_j$. When the NTG model is used, the set of model equations is imposed on the cell level and the local solid and electrolyte potentials are not known. Thus in this case Eq. 12 is applied in its integral form as

$$q = \left[ J\left(\eta - T\frac{\partial U}{\partial T}\right) + \frac{J^2}{\sigma^{eff}} \right] \frac{1}{h} \tag{13}$$

where $\eta$ is the cell overpotential $\left(V_p - V_n - U\right)$, and $h$ is the cell sandwich thickness.

## 2.4 Mechanics

We are primarily concerned with mechanical response of the batteries to external loading, which is one of the major safety concerns. Large deformations of the battery pack that may arise due to crash loads can create internal short circuit that may result in thermal runaway.

Mechanical behavior of the foil materials can be described by the elastic-plastic formulation:

$$\begin{aligned}
&\varepsilon^e{}_{ij} = \frac{1}{E}\left[(1+\nu)\sigma_{ij} - \nu\sigma_{kk}\delta_{ij}\right] \\
&f = \left(S_{ij} - \alpha_{ij}\right)\left(S_{ij} - \alpha_{ij}\right) - 2k^2 = 0 \\
&d\underline{\underline{\varepsilon}}^p = \frac{1}{h}\left\langle d\underline{\underline{S}} : \underline{\underline{n}} \right\rangle \underline{\underline{n}} \\
&d\underline{\underline{\alpha}}^{(m)} = C^{(m)}\left(r^{(m)} d\underline{\underline{\varepsilon}}^p - \underline{\underline{\alpha}}^{(m)} dp\right) \\
&\underline{\underline{\alpha}} = \sum \underline{\underline{\alpha}}^{(m)}
\end{aligned} \tag{14}$$

In the above equations the total strain is the sum of elastic and plastic strains $\varepsilon = \varepsilon^e + \varepsilon^p$ and $dp = \sqrt{d\underline{\underline{\varepsilon}}^p : d\underline{\underline{\varepsilon}}^p}$ is the increment of equivalent plastic strain. Yield surface $f = 0$ is described in terms of deviatoric part ( $\underline{\underline{S}}$ ) of the stress tensor $\underline{\underline{\sigma}}$ with the backstress $\underline{\underline{\alpha}}$ either following Armstrong-Frederick type hardening rule or set to zero for pure isotropic hardening. A similar but more complex model is required for the polymer separators. In addition, the mechanical behavior of composite coatings on the current collectors is not well understood, so effective properties of the composite electrode layers are estimated by experiments on cells and inverse modeling to match experimental response.

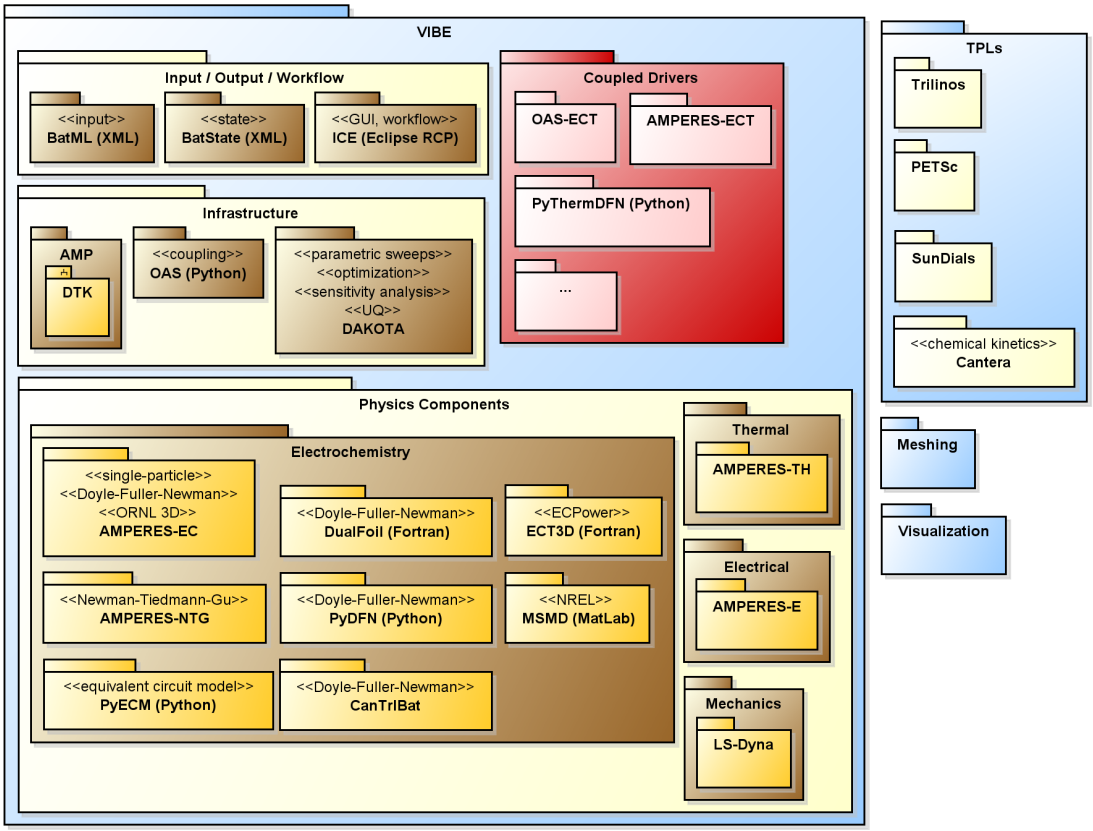


**Figure 2. UML package diagram for the Virtual Integrated Battery Environment (VIBE).**

# 3 Virtual Integrated Battery Environment (VIBE)

VIBE [32] is a new computational environment designed to allow both traditional electrochemistry models such as NTG and DFN and advanced models such as AMPERES to be coupled with thermal and electrical in a fully three-dimensional system so as to more realistically investigate the behavior of complex electrochemical systems. Figure 2 shows the UML package diagram for VIBE, and indicates models currently available. Note that the Python-based Open Architecture Software (OAS) framework is used when loosely coupling components, but tight coupling is also possible within AMPERES, which leverages nonlinear solvers and preconditioners in Trilinos [42], PETSc [43], and SunDials [44]. Two of the combinations of physics models that have been used in analysis include DualFoil +

AMPERES-TH and AMPERES-EC + AMPERES-E + AMPERES-TH. Each combination is controlled by a coupled driver routine, and optimization or parametric studies can be performed using the DAKOTA toolkit [45].

Mechanics is a recent addition to VIBE, necessary for analysis of crush scenarios such as vehicle crashes. This is currently a one-way coupling. A mechanics simulation is performed until separator failure and an internal short circuit is detected. A coupled electrochemistry-electrical-thermal simulation is then performed on the deformed mesh to determine whether thermal runaway occurs.

# 4 Results and Next Steps

To demonstrate the unique capability of VIBE/AMPERES to simulate a scenario requiring three-dimensional effects, we repeat an earlier simulation [32] with an internal short circuit. Lithium manganese oxide was used as an active cathode material with petroleum derived carbon coke as the anode. The electrolyte consisted of LiPF6 salt in non-aqueous mixture of ethylene carbonate (EC) and dimethyl carbonate (DMC) in a poly(vinyl difluoride)-hexafluoropropylene (PVDF-HFP) polymer matrix. Table 1 gives the physical parameters used in the simulation, and Figure 3 shows the solid phase potential for an unrolled cell as described in [37], using a contact resistance converted to a conductance of $10^{-3}$ S/cm. Since this is a single unrolled cell it is a small problem, with only about 70,000 degrees of freedom, so it requires only a few minutes to complete. This demonstrates that AMPERES is robust enough to handle the high discharge rates (100C or more) needed for these scenarios. Note that AMPERES can be used for arbitrarily complex geometries (limited only by ability to generate meshes) and for other chemistries simply by changing model parameters.

Although we have not presented deformation results here, those simulations are underway. However, there are significant challenges with respect to the mechanics of electrodes when crushed and for separator failure models. Both simulations and experiments are under way to develop and validate models for those phenomena.

# 5 Acknowledgements

The research was performed using the resources at Oak Ridge National Laboratory (ORNL), managed by UT-Battelle, LLC, for the U.S. Department of Energy under contract DE-AC05-00OR22725. The authors would like to acknowledge the support of the Vehicle Technologies Program in the Office of Energy Efficiency and Renewable Energy, the National Highway Transportation Safety Agency (NHTSA) of the U.S. Department of Transportation, and the ORNL Laboratory Directed Research and Development (LDRD) program.

**Table 1. Parameters used for AMPERES-EC electrochemistry model in internal short simulation.**

| Symbol | Units | Anode(Carbon) | Separator | Cathode (LiMn2O4) |
|---|---|---|---|---|
| $L_i$ | $\mu m$ | 100 | 52 | 174 |
| $\epsilon_s$ | - | 0.471 | - | 0.297 |
| $\epsilon_e$ | - | 0.503 | 0.724 | 0.630 |
| $\epsilon_f$ | - | 0.026 | - | 0.073 |
| $c_s^{max}$ | $mol/m^3$ | 26390 | - | 22860 |
| $c_s^0$ | $mol/m^3$ | 14870 | - | 3900 |
| $\theta^0$ | - | 0.563 | - | 0.17 |
| $i_0$ | $A/m^2$ | 1.1 | - | 0.8 |
| $D_s$ | $m^2/s$ | $3.9 \times 10^{-14}$ | - | $1.0 \times 10^{-13}$ |
| $k$ | $Am^{2.5}/mol^{3.5}$ | - | - | - |
| $\alpha_a$ | - | 0.5 | - | 0.5 |
| $\alpha_c$ | - | 0.5 | - | 0.5 |
| $c_e^0$ | $mol/dm^3$ | 2.0 | | |
| $D_e$ | $m^2/s$ | $7.5 \times (10)^{-11}$ | - | - |
| $t_+^0$ | - | 0.363 | - | - |
| $\sigma$ | $S/m$ | 100 | - | 3.8 |
| $R_s$ | $\mu m$ | 12.5 | - | 8.5 |
| T | K | 298 | - | - |
| Brugg | - | 3.3 | - | - |

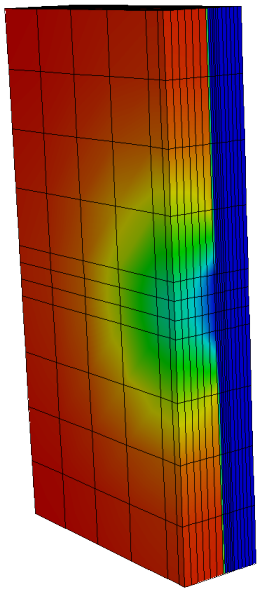

**Figure 3. Solid phase potential due to internal short.**

# References


1. J. B. Goodenough and Y. Kim, Chemistry of Materials **22** (3), 587-603 (2009).
2. G. H. K. A. Pesaran, and M. Keyser, presented at the Proceedings of International Battery, Hybrid and Fuel Cell Electric Vehicle Symposium (EVS-24), Stavanger, Norway, 2009 (unpublished).
3. R. Spotnitz and J. Franklin, Journal of Power Sources **113** (1), 81-100 (2003).
4. K. Smith, G. H. Kim, E. Darcy and A. Pesaran, Int J Energ Res **34** (2), 204-215 (2010).
5. P. P. Mukherjee, S. Pannala and J. A. Turner, in *Handbook of Battery Materials*, edited by C. Daniel and J. O. Besenhard (Wiley-VCH Verlag GmbH & Co. KGaA, Weinheim, 2011), pp. 843-876.
6. W.-J. Lai, M. Y. Ali and J. Pan, Journal of Power Sources **248** (0), 789-808 (2014).
7. F. Ren, T. Cox and H. Wang, Journal of Power Sources **249** (0), 156-162 (2014).
8. G. Ceder, M. Doyle, P. Arora and Y. Fuentes, MRS Bull. **August 2002** (2002).
9. K. Tasaki and S. J. Harris, Journal of Physical Chemistry C **114** (17), 8076-8083 (2010).
10. J. Karo and D. Brandell, Solid State Ionics **180** (23-25), 1272-1284 (2009).
11. X. H. Li, T. O. Drews, E. Rusli, F. Xue, Y. He, R. Braatz and R. Alkire, J. Electrochem. Soc. **154** (4), D230-D240 (2007).
12. W. Pongsaksawad, A. C. Powell and D. Dussault, J. Electrochem. Soc. **154** (6), F122-F133 (2007).
13. J. E. Guyer, W. J. Boettinger, J. A. Warren and G. B. McFadden, Physical Review E **69** (2) (2004).
14. A. Powell and W. Pongsaksawad, in *Simulation of Electrochemical Processes II*, edited by V. G. DeGiorgi, C. A. Brebbia and R. A. Adey (Wit Press/Computational Mechanics Publications, Southampton, 2007), Vol. 54, pp. 43-52.
15. C. Y. Wang, W. B. Gu and B. Y. Liaw, J. Electrochem. Soc. **145** (10), 3407-3417 (1998).
16. W. B. Gu, C. Y. Wang and B. Y. Liaw, J. Electrochem. Soc. **145** (10), 3418-3427 (1998).

17. C. Y. Wang and V. Srinivasan, Journal of Power Sources **110** (2), 364-376 (2002).
18. M. Doyle, T. F. Fuller and J. Newman, J. Electrochem. Soc. **140** (6), 1526-1533 (1993).
19. T. F. Fuller, M. Doyle and J. Newman, J Electrochem Soc **141** (1), 1-10 (1994).
20. G. H. Kim, A. Pesaran and R. Spotnitz, Journal of Power Sources **170** (2), 476-489 (2007).
21. P. Ramadass, B. Haran, P. M. Gomadam, R. White and B. N. Popov, J. Electrochem. Soc. **151** (2), A196-A203 (2004).
22. P. Ramadass, B. Haran, R. White and B. N. Popov, Journal of Power Sources **123** (2), 230-240 (2003).
23. S. Santhanagopalan, Q. Z. Guo, P. Ramadass and R. E. White, Journal of Power Sources **156** (2), 620-628 (2006).
24. S. Santhanagopalan, P. Ramadass and J. Zhang, Journal of Power Sources **194** (1), 550-557 (2009).
25. G. Sikha, R. E. White and B. N. Popov, J. Electrochem. Soc. **152** (8), A1682-A1693 (2005).
26. P. Arora, M. Doyle, A. S. Gozdz, R. E. White and J. Newman, J Power Sources **88** (2), 219-231 (2000).
27. P. Arora, M. Doyle and R. E. White, J Electrochem Soc **146** (10), 3543-3553 (1999).
28. P. Arora, R. E. White and M. Doyle, J Electrochem Soc **145** (10), 3647-3667 (1998).
29. K. Kumaresan, G. Sikha and R. E. White, J Electrochem Soc **155** (2), A164-A171 (2008).
30. M. Dubarry, N. Vuillaume and B. Y. Liaw, Int J Energ Res **34** (2), 216-231 (2010).
31. M. Dubarry, N. Vuillaume and B. Y. Liaw, Journal of Power Sources **186** (2), 500-507 (2009).
32. S. Allu, S. Kalnaus, W. Elwasif, S. Simunovic, J. A. Turner and S. Pannala, Journal of Power Sources **246** (0), 876-886 (2014).
33. W. B. Gu, C. Y. Wang, S. M. Li, M. M. Geng and B. Y. Liaw, Electrochimica Acta **44** (25), 4525-4541 (1999).
34. M. Doyle, J. Newman, A. S. Gozdz, C. N. Schmutz and J. M. Tarascon, J. Electrochem. Soc. **143** (6), 1890-1903 (1996).
35. M. Doyle, T. F. Fuller and J. Newman, J. Electrochem. Soc. **140** (6), 1526-1533 (1993).
36. T. F. Fuller, M. Doyle and J. Newman, J. Electrochem. Soc. **141** (4), 982-990 (1994).
37. V. Srinivasan and C. Y. Wang, J. Electrochem. Soc. **150** (1), A98-A106 (2003).
38. J. Newman and W. Tiedemann, J. Electrochem. Soc. **140** (7), 1961-1968 (1993).
39. H. Gu, J. Electrochem. Soc. 130 (7), 1459-1464 (1983).
40. S. Allu, S. Pannala, J. Nanda, S. Simunovic and J. A. Turner, ECS Meeting Abstracts **MA2014-02** (1), 34 (2014).
41. D. Bernardi, E. Pawlikowski and J. Newman, J. Electrochem. Soc. **132** (1), 5-12 (1985).
42. M. Heroux et al., ACM Trans. Math. Softw., **31** (3), 397-423 (2005).
43. S. Balay et al., PETSc User Manual, ANL-95/11 – Rev. 3.5 (2014).
44. A. C. Hindemarsh et al., ACM Trans. Math. Softw., **31** (3), 363-396 (2005).
45. M. S. Eldred et al., DAKOTA Ver. 4.0 Ref. Manual (2006).